Proceeding of the IEEE
International Conference on Robotics and Biomimetics
Dali, China, December 2019

A High Resolution Image Mosaic Method Based on Camera Calibration for Tunnel Patrol Robot System

Fu Ziqiu[1], Wang Zehua[2], Yu Chen[2], Liang Dan[1], Liang Dongtai[1]

[1]*Faculty of Mechanical Engineering and Mechanics*
Ningbo University
Ningbo, Zhejiang Province, 315211, China
{1711081019 & liangdongtai & liangdan}@nbu.edu.cn

[2]*Ningbo Quanhang Machinery Tech. Co., Ltd*
Ningbo, Zhejiang Province, 315000, China
{wzh & yc}@qh-mechinery.com

***Abstract* - Aiming at the problem of complicated process and limited scope in visual inspection of tunnel defects, a high resolution image mosaic method based on camera calibration for tunnel patrol robot system is proposed. Patroling on the specific track with a high resolution image mosaic module in the tunnel, the designed mobile robot greatly simplifies the defect detection process, and saves a lot of manpower and material resources by using the cylindrical image mosaic method based on fast camera calibration. Through the fast and accurate calibration process, the high resolution panoramic image of the tunnel is obtained without scene constraints, which is beneficial for subsequent comprehensive defect detection. The experimental results show that the camera calibration for high resolution image mosaic system could be done accurately and quickly with tunnel patrol robot run steadily in door and tunnel scenes, and the process of image mosaics is short in time, with high mosaics accuracy and good imaging effect, and strong robustness.**

Index Terms - Mobile Robot; Tunnel Patrol Robot; Camera calibration; Cylindrical projection

I. INTRODUCTION

Road tunnel defect detection plays an important role in engineering application management, which vastly influences the application quality of highway tunnel engineering and the treatment of diseases. Image detection technology has developed rapidly in recent years because of its non-contact measurement between the surface of the tunne, and the images collected by the network transmission server can be analyzed, which has a good application prospect.

David Redman and Nectria Diamanti used a higher resolution ground-coupled geological radar to obtain the geometrical characteristics of the tunnel defective cracks, and the finite difference method is proposed in order to evaluate the crack characteristics quantitatively, which is not only quite accurate in terms of positioning, but also shows a greatly improvement in accuracy [1]. The "Digital Highway Data Vehicle" (DHDV), a real-time pavement crack measurement system developed by American universities, takes the lead of road defect detection. The proposed system is applied by using the captured high resolution road image through the CCD camera mounted on the vehicle to locate the crack information, and the distance measuring device (DMI) to collect the distance information [2]. Jinghang Cen etc. [3] proposed a method to avoid complex preprocessing of input images, which effectively improves the accuracy of recognition. Yichang Tsai et al. has proposed a crack detection method based on the minimum path, and the method only needs one crack point to track all the remaining crack images, but the crack points need to be manually selected, which is random and has the error of manual intervention [4]. In order to solve this problem, Qingquan Li et al. proposed a method based on seed growth to detect crack images, which can selects the starting and ending points of the tunnel crack automatically [5].

However, there are some problems in the above visual detection methods, such as cumbersome process, low efficiency, and limited range. To this end, a high resolution image Mosaic system for tunnel patrol robot is designed. Through the proposed multi-scene blast method based on fast camera calibration, the high resolution panoramic image of the tunnel is obtained. The field of view information effectively solves the problem of limited detection range. The system is mounted on a mobile robot and can be patrolled on specific tracks in the tunnel, which greatly simplifies the inspection process and improves the efficiency. The experiment proves that the system can accurately and quickly complete the camera calibration in indoor and tunnel scenes. The image stitching process takes a short time with high stitching precision, good imaging effect, and strong robustness. The robot equipped with the system can operate stably in tunnel, and provide a highly favorable basis for comprehensive defect detection of structures such as tunnels.

II. TUNNEL PATROL ROBOT SYSTEM DESCRIPTION

The tunnel patrol robot system designed is shown in Figure 1. The high resolution camera is equipped with a turntable and a focusing device that is modularly installed in the mobile inspection robot. The low-power embedded central processor is used to process the image data collected by the camera. Information and data transmission through a complete network system. It's using a standard three-layer network architecture, which is a complete system.

1) The internal communication layer of camera acquisition and robot motion control based on embedded system.

2) Each module in the vision patrol robot communicates with the network server through the built-in 4G router.

3) The main control room establishes the network communication control layer between the server, client and mobile device through Ethernet.

978-1-7281-6321-5/19//$31.00 ©2019 IEEE

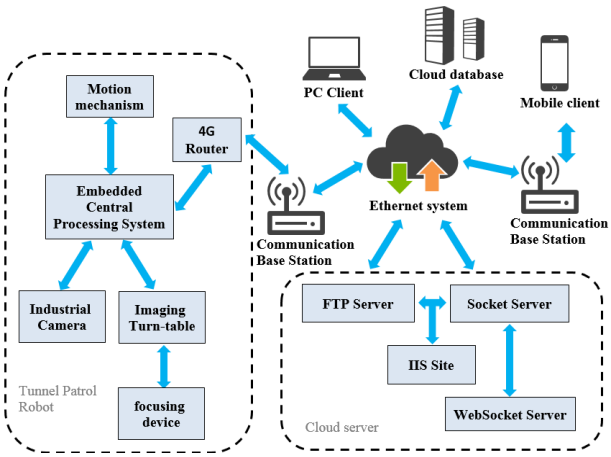

Fig. 1 The Structural Diagram of Tunnel Patrol Robot System

III. CAMERA CALIBRATION ALGORITHM

Image mosaic is a process of combining two or more images with overlapping fields of view in the same scene to produce a seamless panorama or high resolution image [6]. The image obtained by stitching has a larger Wide Field of View (FOV). Image registration is a key step. At present, there are three classic registration methods based on frequency domain, gray-based and feature-based points [7]. Image registration algorithms generally have problems of large computational complexity and low execution efficiency. In this regard, domestic researchers have proposed a method based on camera calibration [8-10], which saves most of the time required for mosaic and achieves higher stitching accuracy.

At present, the image mosaic algorithm based on camera calibration is limited by the scene, and the calibration process is complicated. To this end, the proposed cylindrical image stitching method based on fast camera calibration in multiple scenes can make full use of the feature of high precision extraction of the checkerboard calibration plate, and the pre-processing of corner extraction, refinement and matching for acquired image sequence is performed in order to accurately and quickly get the registration parameters between the images, so that the image mosaic is completed quickly.

A. Calibration Parameter Acquisition

Calibration parameter acquisition can be divided into two processes (Fig. 2). Process 1 first performs corner detection and sub-pixel refinement on adjacent images, and completes corner matching. The matching corner coordinates are used to calculate the homography matrix $\boldsymbol{H}$, combined with the focal length evaluation to obtain the pixel focal length $\boldsymbol{F}$ of each rotation position of the camera. Process 2 uses $\boldsymbol{F}$ to perform cylindrical projection transformation on the source image, and calculates the update $\boldsymbol{H}$ after the cylindrically transformed image is finished with the corner matching, and then obtains the coordinates of the four vertices after the homography transformation of the registration image, and finally obtains the adjustment. The transformed homography matrix $\boldsymbol{H^*M}$ and the translation vector $\boldsymbol{L}$ of the stitched image.

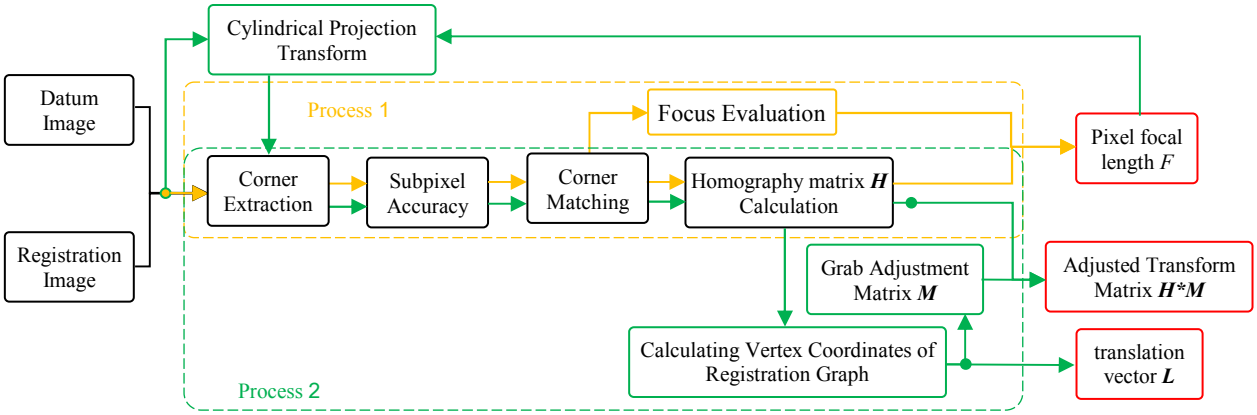

Fig.2 The calibration parameter acquisition flow chart

B. Geometric Model of Imaging

The Pinhole imaging model [11-12] of industrial camera used in the system is built as shown in Fig 3. The reflection is mapped onto the imaging plane after a subject is concentrated by a lens at optical center. In order to facilitate observation and research, it is assumed that the imaging plane is located between the pinhole and the subject, and the imaging direction of the subject is consistent with the actual direction.

The origin O_{cam} of the camera coordinate system in the $X_{cam}Y_{cam}Z_{cam}$ figure is the optical center, and the $X_{cam}Y_{cam}$ plane is parallel to the imaging plane. The distance between the optical center and the optical axis is the focal length f. The image Cartesian coordinate system $x_{img}y_{img}$ and the pixel Cartesian coordinate system uv are all on the imaging plane, and the pixel coordinate value of the image coordinate system origin o_{img} is (u_o, v_o). The conversion relationship between each coordinate system is:

$$\begin{bmatrix} u \\ v \\ 1 \end{bmatrix} = \begin{bmatrix} \gamma_x f & 0 & u_o & 0 \\ 0 & \gamma_y f & v_o & 0 \\ 0 & 0 & 1 & 0 \end{bmatrix} \begin{bmatrix} \boldsymbol{R} & \boldsymbol{t} \\ 0 & 1 \end{bmatrix} \begin{bmatrix} x_w \\ y_w \\ z_w \\ 1 \end{bmatrix} = \boldsymbol{KM} \begin{bmatrix} x_w \\ y_w \\ z_w \\ 1 \end{bmatrix} \quad (1)$$

In the formula $(u, v, 1)^T$ is the homogeneous coordinate of point p in pixel coordinate system, γ_x and γ_y the conversion factor of length and pixel in transverse axis and longitudinal

axis direction, respectively, $\boldsymbol{R}$ is a rotation matrix of 3 × 3, and $\boldsymbol{t}$ is the translation vector of 3 × 1 , $(x_w, y_w, z_w, 1)^T$ is the homogeneous coordinate of three-dimensional point P in the world coordinate system. $\boldsymbol{K}$ is called the internal parameter matrix of the camera and $\boldsymbol{M}$ is the external parameter matrix of the camera.

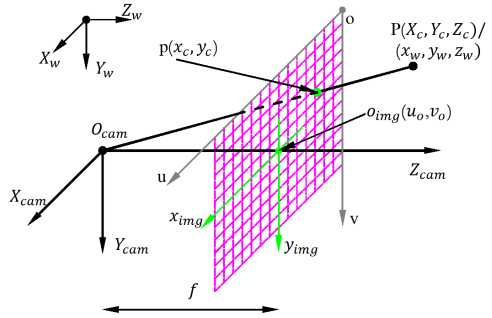

Fig.3 The geometric model of pinhole imaging

C. *Calculation of Homography Matrix*

According to the established imaging model, the mapping relationship between pixel points between image planes needs to be calculated to achieve image registration. The correspondence between planes can be determined by the Homography transform [13]. The transformation between the two image planes in three-dimensional space is shown in Fig. 4. The camera captures image 1 and image 2 (registration image) in two adjacent poses, and the non-singular 3×3 matrix $\boldsymbol{H}$ can be used to describe its mapping relationship. Transforms the registration image plane onto the reference image plane.

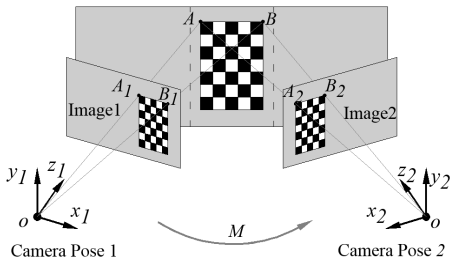

Fig.4 The image projection transformation 3D schematic

On the image 1 and the image 2, the coordinate points $A_1(u_1, v_1, 1)^T$ and $A_2(u_2, v_2, 1)^T$ are respectively obtained, and A_2 figure out the relationship between A_1 and the point can be expressed as:

$$c\begin{bmatrix} u_1 \\ v_1 \\ 1 \end{bmatrix} = \boldsymbol{H}\begin{bmatrix} u_2 \\ v_2 \\ 1 \end{bmatrix} = \begin{bmatrix} h_{11} & h_{12} & h_{13} \\ h_{21} & h_{22} & h_{23} \\ h_{31} & h_{32} & h_{33} \end{bmatrix}\begin{bmatrix} u_2 \\ v_2 \\ 1 \end{bmatrix} \tag{2}$$

In the formula, c denotes the scale factor and $\boldsymbol{H}$ is a homography matrix.

The homography matrix $\boldsymbol{H}$ has only 8 degrees of freedom, which can be solved by direct linear transformation (DLT). The (2) formula is expanded and written into a matrix form as follows:

$$\begin{bmatrix} -u_2 & -v_2 & -1 & 0 & 0 & 0 & u_1u_2 & u_1v_2 & u_1 \\ 0 & 0 & 0 & -u_2 & -v_2 & -1 & v_1u_2 & v_1v_2 & v_1 \end{bmatrix}. \tag{3}$$
$$\begin{bmatrix} h_{11} & h_{12} & h_{13} & h_{21} & h_{22} & h_{23} & h_{31} & h_{32} & h_{33} \end{bmatrix}^T = \boldsymbol{A_i h} = 0$$

In the formula, $\boldsymbol{h}$ is the vector form of matrix $\boldsymbol{H}$, so it is necessary to solve eight unknown variables, which requires four pairs of matching points (each 3 points are not collinear). In order to obtain accurate results, much greater than four point pairs are usually used to calculate. At this point, $\boldsymbol{A_i}$ in formula (3) becomes a multiline matrix $\boldsymbol{A_i}$. Therefore, it is necessary to solve the overdetermined equation system $\boldsymbol{A_n h} = 0$, which can be solved by homogeneous linear least square method [14], that is, the singular value decomposition (SVD), of $\boldsymbol{A_n}$ can obtain $\boldsymbol{h}$ without solving the equation system, and its value is in the rightmost singular vector corresponding to the minimum singular value of $\boldsymbol{A_n}$. Rearranges $\boldsymbol{h}$ to obtain the homography matrix $\boldsymbol{H}$.

IV. CYLINDRICAL IMAGE STITCHING ALGORITHM

The image stitching process (Fig. 5) is based on the registration parameters got by calibration. Firstly, through the designed adaptive industrial camera focus turntable device, the camera's pose and focal length are sequentially changed according to the preset values and the camera captures the image with performed cylindrical projection transformation. The graph and image transformation processing are performed independently, and the efficiency is improved. After the number of image acquisitions reaches a predetermined value, the drawing ends. Then, the transformed image sequence is sequentially read, and the transformation matrix $\boldsymbol{H} * \boldsymbol{M}$ obtained by the calibration is used for the homography transformation. The intermediate image of the sequence is selected as the reference image, and the rest is the registration image. The translation vector obtained by the calibration $\boldsymbol{L}$ is used to stitching the image, and then the stitched image is eliminated by using the multi-band fusion method. Finally, the merged image update is replaced with a new reference image, which is sequentially fused with the registration image to obtain a panoramic image.

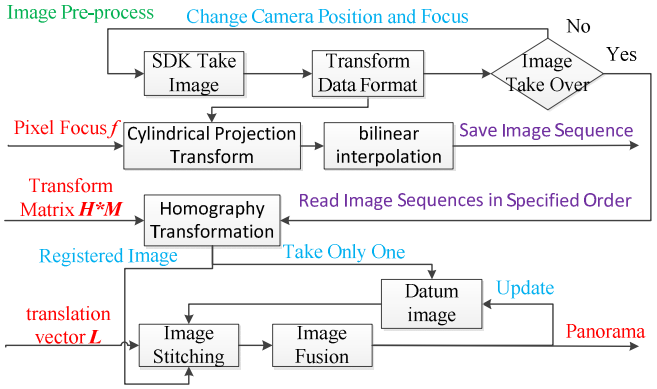

Fig.5 The algorithm framework of image mosaic

A. Cylindrical Projection Transformation

In order to avoid the loss of collinear conditions of imaging during mosaic process, which is advantageous for accurate distance measurement and object recognition. The cylindrical projection transformation [15] is used to project the image onto the cylinder to maintain the visual consistency of the image. The cylindrical projection is shown in Figure 6.

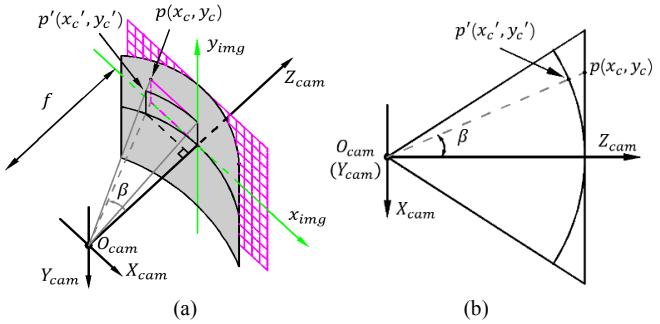

Fig.6 The sketch of Cylindrical projection transformation

In the figure 6(a) is a cylindrical projection in which the imaging plane is a radius with a focal length f, and figure 6(b) is a plan view in the three-dimensional diagram. The point $p\,(x_c,\ y_c)$ is on the image coordinate system, x_c and y_c can be inversely transformed by the formula (2). The point p is transformed to $p'\,(x_c^{'},\ y_c^{'})$ point by cylindrical projection transformation, and the transformation relationship between them can be expressed as:

$$\begin{cases} x_c^{'} = F * arctan\left(x_c / F\right) \\ y_c^{'} = F * y_c / \sqrt{x_c^{\,2} + F^2} \end{cases} \tag{4}$$

In the formula, F is the pixel focal length, $x_c^{'}$ and $y_c^{'}$ are the transverse and longitudinal coordinate values of the image coordinate system on the cylindrical surface.

However, the imaging is on the two-dimensional plane, so the cylindrical image needs to be inversely transformed to the plane. Convert point p' to the camera coordinate system:

$$\begin{cases} X_c^{'} = F * \sin\beta \\ Y_c^{'} = y_c^{'} \\ Z_c^{'} = F * \cos\beta \end{cases} \tag{5}$$

In the formula, $X_c^{'}$, $Y_c^{'}$ and $Z_c^{'}$ is the coordinate value to p' in the camera coordinate system, $\beta = \arctan\left(x_c / F\right)$, according to equations (1) and (2), the inverse transformed pixel coordinates can be obtained:

$$\begin{bmatrix} u' \\ v' \\ 1 \end{bmatrix} = \lambda' \begin{bmatrix} \gamma_x f & 0 & u_o & 0 \\ 0 & \gamma_y f & v_o & 0 \\ 0 & 0 & 1 & 0 \end{bmatrix} \begin{bmatrix} X_c^{'} \\ Y_c^{'} \\ Z_c^{'} \\ 1 \end{bmatrix} \tag{6}$$

In the formula, $\lambda' = 1/\ Z_c^{'}$, $\left(u', v', 1\right)^T$ is the pixel homogeneous coordinate of the point p in the imaging plane, and $\left(X_c^{'}, Y_c^{'}, Z_c^{'}, 1\right)^T$ is the homogeneous coordinate of the point p' in the camera coordinate system.

There are a large number of non-integer values for the u' and v' values of the original image after cylindrical projection transformation and inverse transformation to the plane, and the coordinate requirements of the image points are integers. Using the bilinear interpolation method in [16], the corresponding coordinate values before and after image transformation are solved, the matching of pixel points is completed, the image burr is removed, and a good imaging effect is achieved. The image after cylindrical projection transformation is shown in Fig. 7.

Fig.7 The sketch of Cylindrical projection transformation

B. Image Stitching

The adjacent images are in the same plane after perspective transformation. Using the calibrated translation vector, all the pixels of the registration image are translated, and the corresponding pixel points are coincident and spliced with the reference image. The unfused image is stitched as shown in Fig. 8. The red frame in the figure is the boundary contour of the registration map after perspective transformation, which is located at the specified stitching position after adjustment and translation transformation.

The rightmost image is selected as the reference image, while the image registration image adjacent to the left side is stitched to the reference image by using the calibrated translation vector. The stitched image is fused and updated to the reference image, and the above process can be repeated to complete the image stitching process.

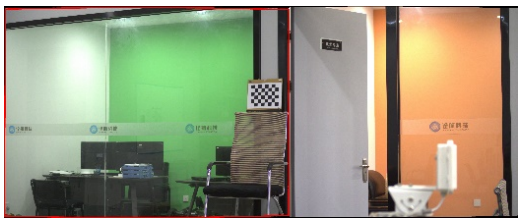

Fig.8 The diagram of Image overlay

C. Image Fusion

The high frequency portion (image detail portion) of the image is significantly blurred when there is a slight misalignment between the overlapping portions of the image through weighted feathering method. Therefore, according to the multi-band fusion method proposed by Brown and Lowe [17], the Laplacian Pyramid (LP) is used to decompose the images to be stitched into different spatial frequency bands and merge them on each spatial frequency layer to keep features

and details on each frequency band to be preserved and fused together.

The fusion process is shown in Fig. 9. Firstly, the Laplacian pyramid is obtained by subtracting the extended image (completing the up-sampling and Gauss convolution) of the upper layer from each layer of the Gauss pyramid. Then the same layer of LPs in the overlapping area are combined by weighted averaging. Finally, the merged LP is extended from the top layer, and the extended image is added to the merged LP image of the next layer to obtain the fused image of the next layer, and the image reconstruction is completed layer by layer.

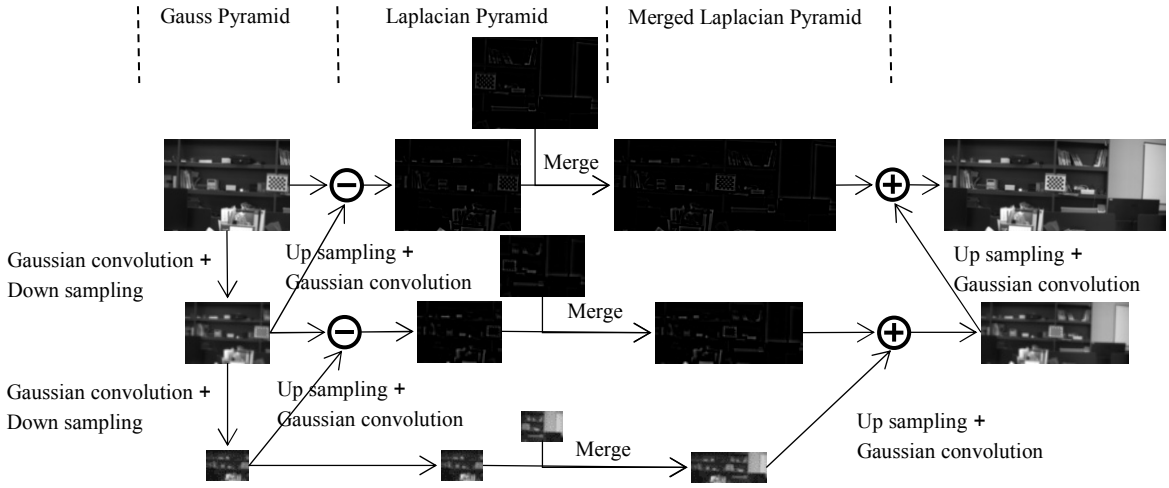

Fig.9 The sketch of multi-band fusion

V. Experimental Results and Analysis

In order to test the feasibility of the system, Hangzhou Wenyi Tunnel before opening to traffic is taken as the experimental scene (Fig. 10). The tunnel is an important part of the Hangzhou "ring, third and fifth horizontal" urban expressway network system, and the traffic flow is large. The daily manual inspection in the tunnel brings personnel safety risk and affects the traffic capacity of the road network. The automatic inspection can gradually replace manual detection and the above problems can be solved by applying the high resolution image mosaic system in Hangzhou Wenyi Tunnel. The mobile inspection robot equipped with high resolution camera module moves back and forth on the fixed track. The image sequence is obtained by the designed image acquisition device, the mosaic algorithm is executed in the CPU system, and the panoramic image of the tunnel is transmitted to the server through the network system layer for detection.

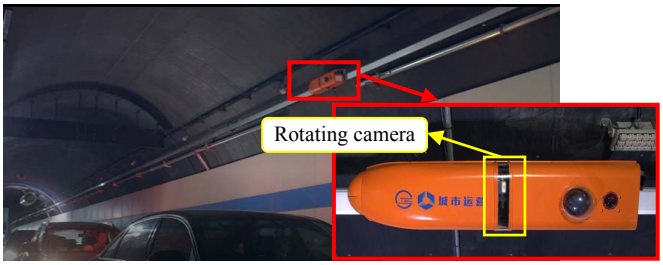

Fig. 10 The application Scene Physical Map of Wenyi Tunnel in Hangzhou

A. *Construction of the experimental system*

The whole image mosaic system is modular and built on a low-power embedded platform (Fig. 11) to make it more flexible and universal. In order to facilitate the experimental analysis, the system is independent. The embedded platform not only performs the bottom control of steering gear motion and camera drawing, but also realizes the camera calibration and image stitching algorithm under Linux as the upper computer. At the same time, it also realizes the communication of each functional module through serial port and ROS (Robot Operating System), so as to realize fast camera calibration and is suitable for a variety of scenes.

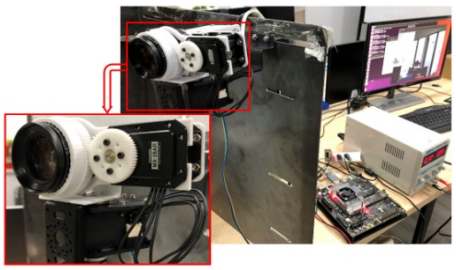

Fig.11 Experimental platform

In this experiment, a set of adaptive focusing device for industrial camera is also designed. The external gear of the lens focusing ring engages with the gear on the steering gear turntable. The steering gear is fixed on the camera frame with L-shaped connectors, and the whole device rotates with the turntable. This device can be adaptively focused by embedded platform to solve the problem of insufficient depth of field of industrial camera.

The low power embedded platform is equipped with ARM Cortex-A57 kernel, the resolution and frame rate are 4096x3000 and 9fpsrespectively, with focal length 25mm industrial focal lens, the minimum angle of steering gear is 0.088 °, the no-load rotating speed of turntable and focusing steering gear is 63rpm and 55rpm, and the static torque is 6.0N.m and 2.5Nm, respectively. The structure is printed in 3D and machined in sheet metal.

B. *Stitching results*

The results of the mosaic through the experimental platform are shown in Fig. 12. In the figure, (a) and (b) are the panoramic images formed by the mosaic of multiple images in the indoor and tunnel scenes respectively. The calibration has been completed in advance, and the mosaic related parameters are as shown in Table 1. It shows that the calibration process is simple and fast, and the mosaic process is completed by the embedded system at one time. After three months of continuous testing, the experimental platform can stabilize the accurate image stitching through the calibrated registration parameters, which shows that the proposed system has strong robustness.

TABLE I

THE PARAMETERS OF IMAGE MOSAIC PROCESS

Name	Parameter
Single image resolution	1.23 Million pixels
View angle of single image（D*H*V）	22° * 36°* 30°
focal length	25mm(Adjustable)
Fixed rotation angle of camera	18°
Image overlap	about 22%
Number of images to be stitched	8

C. *Convergence time comparison analysis*

On the premise that the hardware system has completed the calibration of the camera, it takes 0.83 s for each picture of 12 million pixels. The process includes the rotation of the turntable, the focus of the steering gear and the soft triggering of the camera SDK. Time 1.24s. From the start of the mosaic command to the completion of a complete set of mosaic process a total of 9.64 s (take 8 pictures as an example), the time used in each part is shown in Figure 13. The entire mosaic process is performed independently by multiple nodes, and each part does not affect each other.

Under the same hardware equipment and image data conditions, compared with the [Synthesis [4] using Opencv and [17] SIFT-based stitching method (as shown in Table 2), the data in the table is spliced by two adjacent images respectively. Out, each set of data is the average of 10 experiments.

TABLE II

IMAGE MOSAIC SPEED COMPARISON

	Article method /s	Opencv /s	based Sift Method /s
Image1r_2l	0.1857	1.3945	11.9374
Image2r_3l	0.1773	1.8812	9.1451
Image3r_4l	0.1981	1.3327	6.7098
Image4r_5l	0.1804	1.3343	7.2453
Image5r_6l	0.1851	1.8821	10.1633
Image6r_7l	0.1879	1.5326	7.7876
Image7r_8l	0.1834	1.3769	6.8534

Due to the high resolution of the mosaic source image, the amount of calculation in the mosaic process is large, and the time consuming is relatively long. Experiments were carried out with a low-resolution CCD camera. The two images with a resolution of 640 x 360 pixels were only 0.0113s, and the Opencv stitching method and the SIFT-based stitching required 0.2321s and 0.7863s, respectively. In summary, under the same hardware equipment and image data conditions, two images of 4096×3000 pixels are spliced, the average time of Opencv is 1.533s, and the average time of mosaic method based on SIFT is 8.5488s. The average time consumption of this method is 0.1854s, significantly faster than Opencv and SIFT-based mosaic methods.

Due to the complexity of the image stitching algorithm in Opencv, a large number of calculations are required for the detection of feature points between images, matching and filtering, and finding the optimal stitching line. Therefore, it takes a lot of time; The registration between images is more accurate, but the number of feature points detected during image feature detection is huge, and the image registration process takes a long time. However, the method of this paper only needs to perform camera calibration to quickly obtain the stitching registration parameters, which can then be calibrated. Parameter registration images greatly improve image stitching speed. The mosaic speed of this method is 8 times that of Opencv, and the mosaic method based on SIFT is 45 times faster, which has a very large improvement.

(a)

(b)

Fig.12 The stitching results. (a)The mosaic image in indoor; (b) The mosaic image in tunnel

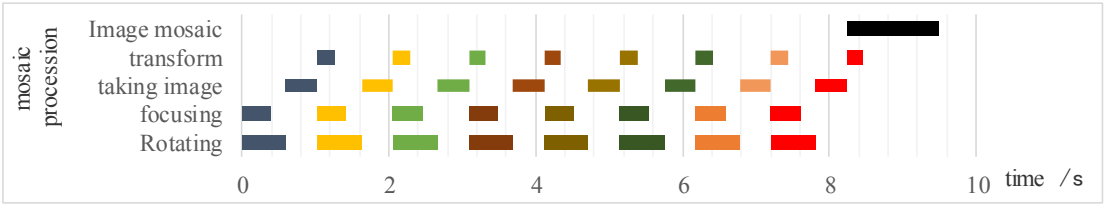

Fig.13 The time bar chart of mosaic process

D. *Comparison and analysis of mosaic accuracy*

The mosaic of the cylinderless projection transformation is shown in Fig. 14, and the result is obtained by stitching fusion of five images. Image stitching directly through the homography transformation will accumulate the effect of scale tilt expansion, and the image after mosaic is seriously distorted, and the imaging effect is extremely poor.

Comparing with Fig. 12, it can be seen that the result of cylindrical mosaic is basically no distortion, and the visual consistency can be better maintained. The multi-band fusion method makes the seams naturally connect, without ghosting and shifting, and has better imaging effects, which can meet the actual needs.

Fig.14 Remove cylindrical projection transformation stitching results

VI. CONCLUSION

The image mosaic method based on camera calibration is not affected by environmental lighting conditions and has strong robustness without losing precision. Using calibration parameters to replace the image registration process can effectively reduce the time required for image mosaic. The cylindrical image mosaic method of fast camera calibration based on chessboard lattice is proposed in this paper, on the basis of which the calibration process is simplified, the calibration is convenient and fast, and is not limited by the scene. The cylindrical projection transformation is used to splice the image on the cylindrical surface, which can maintain visual consistency and has a good imaging effect. The feasibility of the proposed method is verified by the experimental analysis in indoor and tunnel (no characteristic points) scenes. The experimental results show that this method can obtain calibration parameters quickly and accurately. Compared with other image stitching methods, the stitching time is less, there is no double shadow and shift phenomenon, and it has higher accuracy. The tunnel patrol robot with the image mosaic system can run stably, which not only provide accurate and reliable high resolution image information in the tunnel, but also provide a very favorable basis for defect detection. It has important theoretical and engineering application value for regular or routine inspection and health diagnosis of tunnel and other structures.

REFERENCES

[1] Diamanti N , Redman J D , Giannopoulos A . A study of GPR pavement crack responses using field data and numerical modelling[C]// 13th International Conference on Ground Penetrating Radar, GPR2010. IEEE, 2010.
[2] Song Jun. Concrete Crack Detection Algorithm Research Based on Digital Image [D]. 2013.
[3] Cen J, Zhao J, Xia X, et al. Application Research on Convolution Neural Network for Bridge Crack Detection[J]. 2017.
[4] [4] Tsai Y , Kaul V , Yezzi A . Automating the crack map detection process for machine operated crack sealer[J]. Automation in Construction, 2013, 31:10-18.
[5] Zhang D , Li Q , Chen Y , et al. An Efficient and Reliable Coarse-to-fine Approach for Asphalt Pavement Crack Detection[J]. Image and Vision Computing, 2016:S0262885616302153.
[6] Adel E , Elmogy M , Elbakry H . Image Stitching based on Feature Extraction Techniques: A Survey[J]. International Journal of Computer Applications, 2014, 99(6):1-8.
[7] Seo S, Jeonz S, Lee S. Efficient homography estimation method for panorama[C]// Frontiers of Computer Vision. IEEE, 2013:209-212.
[8] Zhang Jinling, Sun Hanxu, Jia Qingxuan, et al. Image Mosaic Algorithm Based on Camera Calibration[J]. Journal of North University of China, 2008, 29(6):575-579.
[9] Wang Dong, Liu Fengying, Chen Tianen, et al. The method of cylinder panoramic image mosaic based on camera calibration parameters[J]. Science of Surveying and Mapping, 2016, 41(7):150-154.
[10] Ma Jialin, Zhang Jinming, Sun Weixin, et al. Research on Panoramic Image Mosaic Method Based on Camera Calibration[J]. Journal of System Simulation, 2017(5):1112-1119.
[11] Zhang Z . Flexible camera calibration by viewing a plane from unknown orientations[C]// Seventh IEEE International Conference on Computer Vision. IEEE, 1999.
[12] Hartley R, Zisserman A. Multiple view geometry in computer vision[J]. Kybernetes, 2008, 30(9/10):1865 - 1872.
[13] Chuan Z , Long T D , Feng Z , et al. A planar homography estimation method for camera calibration[J]. 2003.
[14] Lenth R . Least-squaresmeans: TheR package lsmeans[J]. Journal of Statistical Software, 2016, 069(1):1-33.
[15] Yuan X, Zhou Q, Gong L, et al. High-Speed Simultaneous Image Distortion Correction Transformations for a Multicamera Cylindrical Panorama Real-time Video System Using FPGA[J]. IEEE Transactions on Circuits & Systems for Video Technology, 2014, 24(6):1061-1069.
[16] GUO Haixia，GUO Hailong，XIE Kai. Improved bilinear interpolation algorithm based on edge information[J]. Computer Engineering & Applications, 2011, 47(31):171-174.
[17] Brown M , Lowe D G . Automatic Panoramic Image Stitching using Invariant Features[J]. International Journal of Computer Vision, 2007, 74(1):59-73.

OTHER INFORMATION

Project supported by National Natural Science Foundation of China (51805280), the Public Technology Application Project of Zhejiang (2017C31094) and the Natural Science Foundation of Zhejiang (LQ18E050005)